

Graphical Abstract

Addressing prior dependence in hierarchical Bayesian modeling for PTA data analysis II: Noise and SGWB inference through parameter decorrelation

Eleonora Villa, Luigi D'Amico, Aldo Barca, Fatima Modica Bittordo, Francesco Alì, Massimo Meneghetti, Luca Naso

Highlights

Addressing prior dependence in hierarchical Bayesian modeling for PTA data analysis II: Noise and SGWB inference through parameter decorrelation

Eleonora Villa, Luigi D'Amico, Aldo Barca, Fatima Modica Bittordo, Francesco Alì, Massimo Meneghetti, Luca Naso

- Research highlight 1 : Implementation of Hierarchical Bayesian modeling and integration of flow-guided nested sampling into Pulsar Timing Array Bayesian inference pipelines
- Research highlight 2 : Decorrelation in the parameter space implemented via Normalizing Flows to address prior dependence

Addressing prior dependence in hierarchical Bayesian modeling for PTA data analysis II: Noise and SGWB inference through parameter decorrelation

Eleonora Villa^{a,*}, Luigi D’Amico^b, Aldo Barca^b, Fatima Modica Bittordo^b, Francesco Ali^b, Massimo Meneghetti^c, Luca Naso^b

^a*INAF – Istituto di Astrofisica Spaziale e Fisica Cosmica di Milano (IASF-MI), via Alfonso Corti 12, Milano, 20133, Italy*

^b*Koexai srl, Via Jose Maria Escriva, 6, Catania, 95125, Italy*

^c*Osservatorio di Astrofisica e Scienza dello Spazio di Bologna (INAF-OAS), via Gobetti 93/3, Bologna, 40129, Italy*

Abstract

Pulsar Timing Arrays provide a powerful framework to measure low-frequency gravitational waves, but accuracy and robustness of the results are challenged by complex noise processes that must be accurately modeled. Standard PTA analyses assign fixed uniform noise priors to each pulsar, an approach that can introduce systematic biases when combining the array. To overcome this limitation, we adopt a hierarchical Bayesian modeling strategy in which noise priors are parametrized by higher-level hyperparameters. We further address the challenge posed by the correlations between hyperparameters and physical noise parameters, focusing on those describing red noise and dispersion measure variations. To decorrelate these quantities, we introduce an orthogonal reparametrization of the hierarchical model implemented with Normalizing Flows. We also employ *i-nessai*, a flow-guided nested sampler, to efficiently explore the resulting higher-dimensional parameter space. We apply our method to a minimal 3-pulsar case study, performing a simultaneous inference of noise and SGWB parameters. Despite the limited dataset, the results consistently show that the hierarchical treatment constrains the noise parameters more tightly and partially alleviates the red-noise–SGWB degeneracy, while the orthogonal reparametrization further enhances parameter independence without affecting the correlations intrinsic to the power-law modeling of the physical processes involved.

Keywords: Hierarchical Bayesian modeling, Pulsar Timing Array, Nested sampling, Normalizing Flows, Decorrelation in the parameter space

1. Introduction

Understanding physical phenomena through parameter inference from observational data is a core task in modern astronomy. To account for poorly constrained effects, unmodeled physics, noises, and/or some systematics, it is standard practice to introduce so-called nuisance parameters that capture unknown or subdominant contributions. Although not of direct scientific interest, nuisance parameters are often correlated with the target physical parameters, and this gives rise to

^{*}Corresponding author.

Email address: `eleonora.villa@inaf.it` (Eleonora Villa)

degeneracies in the posteriors. As a result, the inferred values of the parameters of interest may be biased or misrepresented, depending on the modeling chosen for the nuisance contributions. This issue is particularly critical when the data lack the constraining power to disentangle nuisance effects from the parameters of interest.

This problem plays a particularly important role in the context of Pulsar Timing Arrays (PTA) analyses. PTA experiments measure the times of arrival (TOAs) of radio pulses emitted by highly stable millisecond pulsars. These measurements are modeled using a deterministic timing model that accounts for effects such as the pulsar spin evolution, astrometric parameters, and proper motion. Any deviation between the observed TOAs and the timing model predictions — referred to as timing residuals — is attributed to a combination of noise processes and potential gravitational wave signals. Recently, PTA experiments across the world have reported evidence for a stochastic gravitational wave background (SGWB), marking a major milestone in low-frequency gravitational wave astronomy, see Agazie et al. (2023), EPTA Collaboration et al. (2023), Xu et al. (2023), and Reardon et al. (2023). However, extracting meaningful information from the SGWB signal critically depends on accurately modeling the various noise contributions in the data, making this an especially delicate task. PTA analyses rely on modeling multiple sources of noise, such as intrinsic red noise and dispersion measure (DM) variations, which are both modeled as power-law signals and described by two parameters each, the \log_{10} of the amplitude and the spectral index γ , for each pulsar. The same kind of parameters describe the SGWB signal too, as it is modeled as a single power law common process across all the pulsars in the array. In a single-pulsar analysis, each pulsar represents a single realization of data with respect to the noise stochastic processes. The crucial point here is that it could happen that a certain type of noise is not significantly detectable in the data of a single pulsar whereas it becomes detectable in the data of the full array: this means that the entire array of pulsars represents a different realization of data with respect to the same noise parameters. By contrast, since the SGWB is modeled as a single common signal shared across all pulsars, the full array provides a single realization with respect to the SGWB parameters, unlike the case for noise parameters. The above considerations imply that using the results of single-pulsar analyses — such as assuming the absence of a given noise process — as priors in a full-array analysis can be problematic. It is not only an example of the so-called circular use of data but it also applies a prior derived from the wrong statistical realization. The discrepancy between the statistical description of the noise processes in the single pulsars and their statistical description in the entire array may accumulate across pulsars and lead to biased inference, e.g. it may introduce systematic errors in the inferred values of $\log_{10} A$ and γ for the power law model of the SGWB. This is especially crucial for the pulsar red noise which is highly correlated with the SGWB, both being low-frequency stochastic processes modeled in the same way. The solution of this problem is then clear: the distribution of the noise parameters should be parametrized for each pulsar and inferred simultaneously with that of the two SGWB parameters in the analysis of the full array. This means that we have to choose a prior for all the parameters to infer, including noise priors. To account for the uncertainty in the noise distributions we parametrize noises prior by introducing an additional hierarchical prior encoded in additional parameters, called hyperparameters. They describe the distribution of noise properties across the array and act as nuisance parameters in the inference problem. We remark that the hierarchical Bayesian modeling becomes necessary in PTA analyses, as it allows for the correct inference of both the astrophysical signal of interest, such as the SGWB, and the population-level noise properties encoded in the hyperpriors. All the above considerations were recently pointed out, although with slightly different approaches, in Goncharov and Sardana (2025), van Haasteren (2024a), and van Haasteren (2024b). For a discussion about previous literature implicitly showing this problem,

referred to as *prior misspecification*, also see Goncharov and Sardana (2025).

At this point, a well-known aspect of Bayesian modeling becomes relevant: posterior distributions can be significantly influenced by the choice of priors. This problem, known as *prior dependence* or prior-driven projection effects, affects every level of hierarchical modeling. Various strategies have been explored to address this issue in many different contexts. In general, one approach is to impose physically motivated priors, for instance informed by simulations or empirical models. Another possibility is to employ priors considered "non-informative", such as uniform or Jeffreys priors. Yet these choices come with their own limitations: uniform priors may implicitly encode arbitrary assumptions e.g. on prior bounds, and Jeffreys priors, although invariant under reparametrization, are often impractical in complex analyses. While uniform priors are of standard use in pulsar astronomy, in Laal et al. (2025) is proposed the use of Jeffreys-like prior for all the red processes (red noise and SGWB) in the full array analysis. At the level of hierarchical Bayesian modeling, the *prior dependence* can be formulated as follows: the inference of the parameters of physical interest - the noises and the SGWB parameters in the case of PTA - is sensitive to the specific prior that we choose - the hyperprior for the noises in the case of PTA. This is recovered in the work by Goncharov and Sardana (2025), where the authors resolve *prior misspecification* by introducing hyperparameters for red and DM noises. Then, they employ a novel numerical marginalization technique over hyperparameters for the inference of physical parameters of the red and DM variation noises but still their results are sensitive to the choice of the lower-level prior of the noises.

In this work, we use the hierarchical Bayesian description but we pursue a different strategy. Rather than proposing specific hyperpriors or marginalizing over hyperparameters, we develop a reparametrization of the model designed to decorrelate hyperparameters from the physical parameters of the red and DM variation noises which aims to mitigate *prior dependence*. Our methodology builds on the principle of parameter orthogonalization, first established in a formal statistical framework by Cox and Reid (1987), who demonstrated that orthogonal parameterizations can achieve approximate conditional inference and reduce parameter correlations. This foundational concept was subsequently extended by Tibshirani and Wasserman (1994), who explored various theoretical and practical aspects of statistical model reparameterization, and by Christensen et al. (2006), who showed that orthogonal transformations significantly enhance MCMC sampling efficiency. More recently, Paradiso et al. (2025) applied a non-linear orthogonalization technique using Generalized Additive Models (GAMs) to the Effective Field Theory of large-scale structure in cosmology. They showed that decorrelating cosmological and nuisance parameters makes the posterior less sensitive to the choice of nuisance priors. Their results agree with the theoretical predictions of Papaspiliopoulos et al. (2007), who established a comprehensive framework demonstrating that orthogonal parameterizations in hierarchical models naturally lead to more robust inference with decreased prior sensitivity. Our contribution consists of applying this approach to the hierarchical structure of the PTA noise model. The idea is conceptually quite simple: we orthogonalize the hyperparameter vector by removing its projection onto the subspace spanned by the physical noise parameters. The resulting orthogonal complement vector constitutes our new decorrelated hyperparameter vector, which is, by construction, decorrelated from the physical parameters. To implement the orthogonal transformation we employ a 2-steps Normalizing Flows algorithm that learns how to pass from one parameter set to the other. We then systematically evaluate how this reparameterization affects the posterior distributions of the noise parameters. For Bayesian inference, we use **i-nessai**, a flow-guided nested sampler presented in Williams et al. (2023), which updates the previous version of the algorithm, see Williams et al. (2021) and Williams (2021). **i-nessai** leverages Normalizing Flows to navigate complex, high-dimensional parameter spaces

efficiently, making it particularly advantageous for computationally intensive likelihood evaluations characteristic of PTA analyses. The method provides substantial computational acceleration compared to the standard PTMCMC sampler traditionally used in PTA studies, Villa et al. (2025).

The structure of the paper is as follows. In Section 2 we introduce the setup PTA data analysis and outline the role of hierarchical Bayesian modeling. In section 3 we summarize the key steps of the reparametrization procedure and its implementation. A full and detailed description is provided in our companion paper D’Amico et al. (2025). In Section 4 we discuss the results obtained from a minimal 3-pulsar case study, illustrating the main effects of the hierarchical modeling and reparametrization on noise and SGWB inference. Finally, Section 5 provides our conclusions and perspectives for future applications.

2. PTA data analysis set up

In PTA experiments the primary observables are the times of arrival (TOAs) of pulses from an ensemble of millisecond pulsars. These TOAs are compared to a deterministic timing model that accounts for pulsar spin-down, astrometric, and (where relevant) binary parameters. The differences between the observed TOAs and the predictions of the timing model define the timing residuals, which contain both astrophysical signals and various noise contributions. The residuals can be decomposed into several components: (i) the timing model itself, which is linearized around best-fit parameters; (ii) intrinsic red noise, a correlated stochastic process associated with each pulsar individually; (iii) a stochastic gravitational wave background, modeled as a red process correlated across all pulsars according to the Hellings–Downs correlation; (iv) DM variations noise, due to the frequency-dependent propagation of the radio signal through the ionized interstellar medium; and (v) white noise, typically dominated by radiometer noise and possible short-term pulse-phase jitter, both uncorrelated between TOAs. For a detailed description of PTA data model and likelihood, we refer the reader to Chapter 7 of Taylor (2021).

In our hierarchical description of the noise, we focus on intrinsic red noise and DM variations noise. White noise, being uncorrelated with both red processes and the SGWB, is fixed (we set EFAC to unity) and not included in the reparametrization scheme. Our analysis is based on synthetic pulsar timing data generated from the EPTA DR2new parameter files (collaboration et al., 2023). We simulate timing residuals for an array of millisecond pulsars with realistic observational properties: a cadence of 5 days, observation frequencies randomly drawn from $\{500, 900, 1400\}$ MHz, timing uncertainties of $1\ \mu\text{s}$, and a baseline spanning from MJD 52000 to 59000 (approximately 19 years). Using the `libstempo` framework, we inject multiple stochastic processes to construct a realistic test scenario, including intrinsic red noise, dispersion measure (DM) variations, and a stochastic gravitational-wave background (SGWB). All processes are modeled as Gaussian processes with power-law power spectral densities of the form

$$P(f) = \frac{A^2}{12\pi^2} \left(\frac{f}{f_{\text{yr}}} \right)^{-\gamma} f^{-3},$$

where A and γ denote the amplitude and spectral index, respectively. Each process is represented using 30 Fourier components over the frequency range $[10^{-9}, 10^{-5}]$ Hz. For DM variations, the additional chromatic dependence f^{-2} of the timing residuals is accounted for through the Fourier design matrix, rather than explicitly included in the power spectral density. The injected parameters have values: $A_{\text{RN}} = 7 \times 10^{-14}$, $\gamma_{\text{RN}} = 3$; $A_{\text{DM}} = 5 \times 10^{-14}$, $\gamma_{\text{DM}} = 2.3$; $A_{\text{GWB}} = 2 \times 10^{-15}$, $\gamma_{\text{GWB}} = 13/3$.

This formulation is consistent across all red processes and ensures a uniform parametrization of the intrinsic, chromatic, and common signals. The complete probabilistic model is implemented

through `Enterprise`, which constructs the total covariance matrix by combining the individual Gaussian-process components and analytically marginalizing over the linear timing model parameters. For each pulsar, intrinsic red noise and DM variations are described by independent Gaussian processes with parameters $(\log_{10} A_{\text{RN}}, \gamma_{\text{RN}})$ and $(\log_{10} A_{\text{DM}}, \gamma_{\text{DM}})$, respectively. Uniform priors are assigned as $\log_{10} A_{\text{RN}}, \log_{10} A_{\text{DM}} \sim \mathcal{U}(-16, -12)$ and $\gamma_{\text{RN}}, \gamma_{\text{DM}} \sim \mathcal{U}(0, 7)$. The SGWB is modeled as a common Gaussian process shared by all pulsars, with spatial correlations described by the Hellings–Downs overlap reduction function. Its parameters $(\log_{10} A_{\text{GWB}}, \gamma_{\text{GWB}})$ follow the same uniform prior ranges as the intrinsic processes. The likelihood for PTA residuals is modeled as a multivariate Gaussian distribution with a covariance matrix that incorporates the correlations induced by the various processes. Standard PTA analyses marginalize analytically the linear timing model parameters, yielding a reduced likelihood that depends only on the stochastic processes implemented in a single object in `Enterprise`.

3. Parameter decorrelation in hierarchical Bayesian modeling

3.1. Methodology

Here we highlight the essential aspects of the reparametrization procedure, while the complete methodological description can be found in our companion paper D’Amico et al. (2025). Let us start by making the idea of parameter orthogonalization more formal. We consider some physical parameters $\boldsymbol{\vartheta}$ whose prior distribution $\pi(\boldsymbol{\vartheta}|\boldsymbol{\Lambda})$ is parametrized by the hyperparameters $\boldsymbol{\Lambda}$ which in turn are distributed according to their hyperprior $\pi'(\boldsymbol{\Lambda})$, in general different from the distribution π . In our hierarchical framework the total number of physical noise parameters is $n = n_p \times 4$, where $\boldsymbol{\vartheta} = \{\gamma_{\text{RN}}, \gamma_{\text{DM}}, \log_{10} A_{\text{RN}}, \log_{10} A_{\text{DM}}\}$ and n_p is the number of pulsars in the dataset¹. The hyperpriors can be chosen as Gaussian or uniform distributions, with 2 hyperparameters each - mean and standard deviation for the Gaussian prior or lower and upper bounds for the uniform prior -, leading to $m = n_p \times 8$ hyperparameters in total. Our parameter space has therefore $n + m$ dimensions. The joint posterior of all the two-levels parameters is given by, see Thrane and Talbot (2019) and Goncharov and Sardana (2025)

$$\mathcal{P}(\boldsymbol{\vartheta}, \boldsymbol{\Lambda} | \boldsymbol{\delta t}) = \frac{\mathcal{L}(\boldsymbol{\delta t} | \boldsymbol{\vartheta}) \pi(\boldsymbol{\vartheta} | \boldsymbol{\Lambda}) \pi'(\boldsymbol{\Lambda})}{\mathcal{Z}}. \quad (1)$$

In the above equation $\mathcal{L}(\boldsymbol{\delta t} | \boldsymbol{\vartheta})$ is the likelihood and depends on the physical parameters only and \mathcal{Z} is the Bayesian evidence. The hierarchical structure is fully encoded in the parametrized prior term $\pi(\boldsymbol{\vartheta} | \boldsymbol{\Lambda})$ giving the distribution of $\boldsymbol{\vartheta}$ conditional to that of the hyperparameters $\boldsymbol{\Lambda}$, $\pi'(\tilde{\boldsymbol{\Lambda}})$.

The basic idea for the decorrelation is simple: given the hyperparameter vector $\boldsymbol{\Lambda}$ and the subspace generated by the physical noise parameters $\boldsymbol{\vartheta}$, we obtain the decorrelated hyperparameters $\tilde{\boldsymbol{\Lambda}}$ by computing the orthogonal complement of $\boldsymbol{\Lambda}$ with respect to the $\boldsymbol{\vartheta}$ -subspace, effectively removing any linear dependence between the two parameter sets. The required transformation is given by

$$\tilde{\boldsymbol{\Lambda}} = \boldsymbol{\Lambda} - P_{\boldsymbol{\vartheta}} \boldsymbol{\Lambda} = (I - P_{\boldsymbol{\vartheta}}) \boldsymbol{\Lambda}, \quad (2)$$

where

$$P_{\boldsymbol{\vartheta}} \equiv \boldsymbol{\vartheta} (\boldsymbol{\vartheta}^T \boldsymbol{\vartheta})^{-1} \boldsymbol{\vartheta}^T \quad (3)$$

¹The two parameters of the SGWB, $\gamma_{\text{GWB}}, \log_{10} A_{\text{GWB}}$, common to all the pulsars, must be added to this set. However they are not involved in the hierarchical framework. To be precise, the full parameter space has therefore dimensions $n + m + 2$.

is the projector on the subspace spanned by $\boldsymbol{\vartheta}$. Geometrically, this means removing from $\boldsymbol{\Lambda}$ the component lying along the direction of $\boldsymbol{\vartheta}$. As a result, the transformed hyperparameters $\tilde{\boldsymbol{\Lambda}}$ satisfy by construction the orthogonality condition $\boldsymbol{\vartheta}^T \tilde{\boldsymbol{\Lambda}} = 0$. The initial hierarchical structure encodes how physical parameters depend on potentially correlated hyperparameters, along with the hyperparameters own distribution. Our goal is to construct an equivalent representation by using the new $\tilde{\boldsymbol{\Lambda}}$, defined to be orthogonal to the physical parameter directions, along with the corresponding distribution of these transformed hyperparameters. That is, we want to construct the transformation

$$\pi(\boldsymbol{\vartheta}|\boldsymbol{\Lambda})\pi'(\boldsymbol{\Lambda}) \longrightarrow \pi(\boldsymbol{\vartheta}|\tilde{\boldsymbol{\Lambda}})\tilde{\pi}'(\tilde{\boldsymbol{\Lambda}}). \quad (4)$$

The issue with this simple procedure is that the orthogonal projection in Equation 2 does not admit an inverse. As a consequence, the variable change in Equation 4 is ill-defined. We address this issue by directly modeling both $\pi(\tilde{\boldsymbol{\Lambda}})$ and $\pi(\boldsymbol{\vartheta}|\tilde{\boldsymbol{\Lambda}})$ with machine learning generative algorithms that accurately approximate complex or even singular distributions into simpler ones through sequences of invertible mappings. They are called *Normalizing Flows* (NFs) exactly because of their ability to regularize irregular distributions; for reviews and applications in Bayesian inference see Papaspiliopoulos et al. (2007), Rezende and Mohamed (2015), and Kobyzhev et al. (2021). Here we also make use of a special subclass of NFs, especially designed for conditional probability distributions, Trippe and Turner (2018). Our procedure is as follows. We sample from the prior $\pi(\boldsymbol{\Lambda})$, then propagate through the hierarchy to obtain $\boldsymbol{\vartheta}$, and finally compute $\tilde{\boldsymbol{\Lambda}}$ via the projection:

1. draw $\boldsymbol{\Lambda}_i \sim \pi(\boldsymbol{\Lambda})$ for $i = 1, \dots, N_{\text{samples}}$;
2. draw $\boldsymbol{\vartheta}_i \sim \pi(\boldsymbol{\vartheta}|\boldsymbol{\Lambda})$ for $i = 1, \dots, N_{\text{samples}}$;
3. compute $\tilde{\boldsymbol{\Lambda}}_i = (I - P_{\boldsymbol{\vartheta}_i})\boldsymbol{\Lambda}_i$
4. check the orthogonality condition $\boldsymbol{\vartheta}_i^T \tilde{\boldsymbol{\Lambda}}_i = 0$ for the samples.

At this point, two complementary NFs learn the distributions needed for Equation 4 directly from the triples $(\boldsymbol{\vartheta}_i, \boldsymbol{\Lambda}_i, \tilde{\boldsymbol{\Lambda}}_i)$. This dual construction provides the necessary ingredients for Equation 4: by exploiting NFs, we approximate the mapping of Equation 2 and obtain a regularized inverse, all while remaining consistent with the orthogonalization scheme and the hierarchical relation between priors and hyperpriors. This decorrelation should, in principle, ensure that the inference of physical parameters becomes more robust to the choice for the hyperparameter priors. It is important to remark that the sampling procedure is performed from the prior distributions of $\boldsymbol{\Lambda}$ and $\boldsymbol{\vartheta}$, rather than from their posteriors. This choice avoids any form of circular analysis, ensuring that the Normalizing Flows learn the mapping between hyperparameters and physical parameters without being biased by the specific data realization or by the posterior structure of a given dataset.

3.2. Implementation for PTA data analysis

In this section we provide a schematic description of the implementation of our hierarchical framework for PTA data analysis, as pictured in Figure 1. A comprehensive and technical discussion can be found in our companion paper D’Amico et al. (2025).

Normalizing Flows. The orthogonal transformation described in Section 3 is implemented through a two-step NFs architecture that learns the mapping between the correlated and decorrelated representations of the hierarchical model.

The first component, the **push-forward** flow (PF-NF), learns the distribution $\pi'(\tilde{\boldsymbol{\Lambda}})$ of the decorrelated hyperparameters, preserving orthogonality. It is implemented as a Masked Autoregressive Flow (MAF) (Papamakarios et al., 2017), composed of three transformation blocks with masked affine autoregressive layers of 32 hidden units each. This design ensures exact invertibility with

tractable Jacobian computation in $\mathcal{O}(m)$ time, enabling both efficient sampling and accurate likelihood evaluation.

The second component, the ***pull-back*** conditional flow (PB-CNF), learns the conditional distribution $\pi(\boldsymbol{\vartheta}|\tilde{\boldsymbol{\Lambda}})$ of the physical parameters given the decorrelated hyperparameters, preserving the hierarchical structure. It is implemented as a conditional MAF (Trippe and Turner, 2018), where the context $\tilde{\boldsymbol{\Lambda}}$ is injected at each transformation layer. The network consists of three conditional masked affine transformations with shared weights across layers, allowing the model to capture the hierarchical dependence between the two parameter spaces while preserving orthogonality by construction.

Both flows are trained jointly on a dataset of $N_{\text{samples}} = 20000$ realizations drawn from the priors of $(\tilde{\boldsymbol{\Lambda}}, \boldsymbol{\vartheta})$. Training is performed with a mini-batch size of 256, introducing stochasticity that helps avoid poor local minima and enhances generalization. A 90/10 split between training and validation sets is adopted, and an early-stopping criterion selects the model corresponding to the minimum validation loss. The optimization objective is the standard negative log-likelihood used in NF training: the PF-NF maximizes the likelihood of the decorrelated hyperparameters, while the PB-CNF maximizes the conditional likelihood of the physical parameters.

Implementation for PTA data analysis. The reparametrized hierarchical Bayesian framework is implemented through the joint use of `Enterprise` and `i-nessai`: `Enterprise` serves as a likelihood engine, always evaluated exclusively for the physical parameters without altering the internal structure of the PTA class, and in accordance with the hierarchical posterior structure of Equation 1. All prior and hyperprior specifications, both in their original and reparametrized forms, are defined and managed within `i-nessai`. This split implementation allows `Enterprise` to focus solely on the physical model likelihood, while `i-nessai` handles all aspects of hierarchical sampling and reparametrization. The resulting interface provides a modular and extensible framework for hierarchical posterior inference in PTA analyses, readily adaptable to larger or more complex datasets without modifying the internal `Enterprise` architecture.

4. Discussion of the results

In this Section we present the results of our hierarchical Bayesian analysis applied to the simulated PTA dataset introduced in Section 2. We applied the proposed decorrelation scheme within the hierarchical framework to a three-pulsar configuration, performing a simultaneous inference of noise and SGWB parameters. Although such a small array is not sufficient to draw exhaustive quantitative conclusions, it provides a clear and controlled case study that allows us to isolate and highlight the main effects of the hierarchical modeling and reparametrization. Hyperparameters were introduced only for the noise components, namely for the intrinsic red noise and the DM variations, while the stochastic gravitational wave background parameters are left at the standard single-level description. We focus here on the representative pulsar J1744–1134. Analogous results are obtained for the other two pulsars in the array.

As a starting point, we consider the reference runs with fixed, non-hierarchical priors on the noise parameters, i.e. flat priors $\pi(\boldsymbol{\vartheta})$ within the bounds $[-16, -12]$ for $\log_{10} A$ and $[0, 7]$ for γ , as specified in Section 2. This baseline configuration corresponds to the standard PTA inference approach where all noise and signal parameters are treated independently, without introducing hyperpriors $\pi(\boldsymbol{\Lambda})$. The corner plots and marginal posteriors reported here therefore represent the reference posterior distributions against which the hierarchical and reparametrized results will be compared in the following subsections.

Architecture of i-nessai hierarchical models

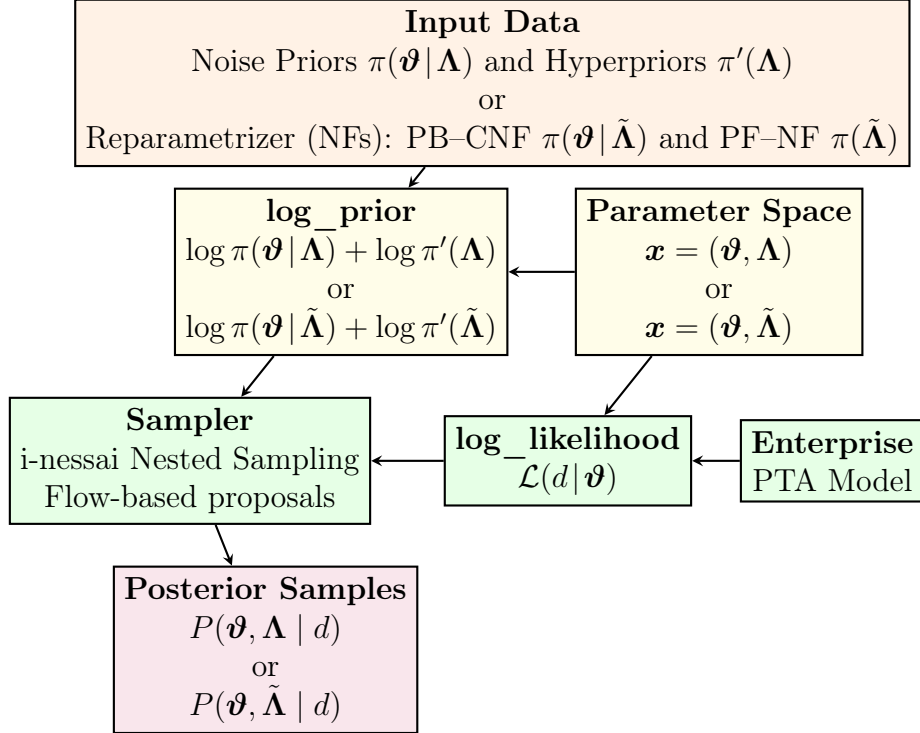


Figure 1: Architecture of the **i-nessai** hierarchical model, shown in both the non-reparametrized (hyperparameters Λ) and reparametrized (hyperparameters $\tilde{\Lambda}$) forms. This implementation handles standard hierarchical Bayesian inference in the two situations: the first with explicit uniform conditional priors $\pi(\vartheta|\Lambda)$ and Gaussian or uniform hyperpriors $\pi'(\Lambda)$; the second with a pair of Normalizing Flows: the push-forward PF-NF encoding $\pi'(\tilde{\Lambda})$ and the pull-back PB-CNF encoding $\pi(\vartheta|\tilde{\Lambda})$. The likelihood is evaluated via **Enterprise** and priors and likelihood feed the sampler **i-nessai** in parallel. The output are the posterior samples.

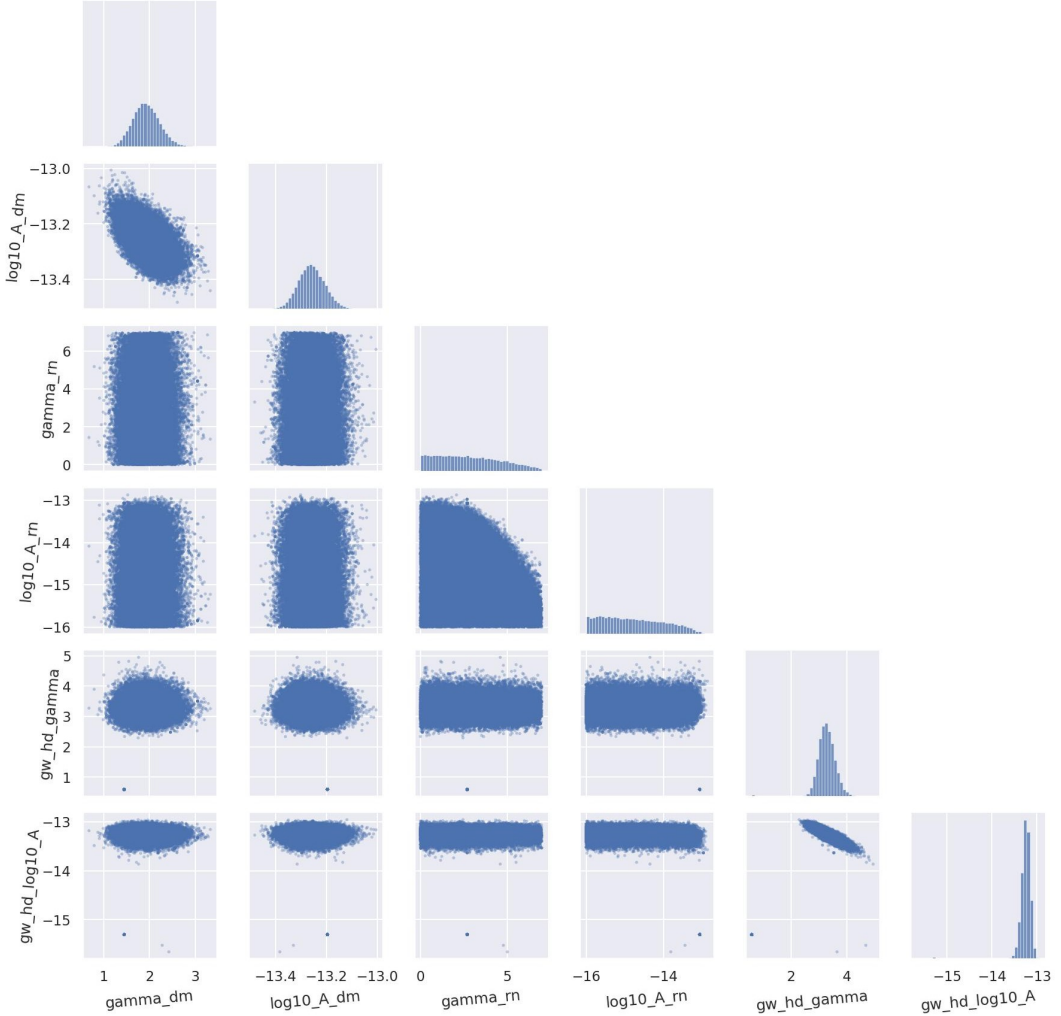


Figure 2: Corner plot showing the 2D-joint posterior distributions of the noise and SGWB parameters for pulsar J1744–1134 under fixed, non-hierarchical priors. The two-dimensional contours display the characteristic anti-correlation between the logarithmic amplitude and spectral index typical of the power-law modeling of both DM variations and SGWB. In contrast, the intrinsic red noise is almost unconstrained in this configuration: with only three pulsars in the dataset, the data provide little sensitivity to individual red-noise parameters, resulting in broad, nearly flat posteriors that indicate the dominance of prior information. These results provide the reference case for assessing the impact of the hierarchical modeling and reparametrization presented in Section 3.1.

The first striking feature visible in Figure 2 is that the intrinsic red noise is practically unconstrained in this configuration, while the SGWB shows the opposite behaviour, with sharply peaked posteriors for both $\log_{10} A$ and γ . This contrast directly reflects the different constraining power of the dataset on individual versus common processes. Since both the red noise and the SGWB contribute power on overlapping low-frequency ranges, the sampler tends to allocate the common signal either to the SGWB or to the individual red-noise terms depending on their prior bounds, number of Fourier components, correlation pattern, and on the number of pulsars in the array. With only three pulsars, the dataset provides limited leverage to disentangle these two sources of correlated noise, and the sampler naturally favors the SGWB component, whose spatial correlation pattern — the Hellings–Downs curve — provides a more distinctive signature. With the common uniform prior range $\log_{10} A \in [-16, -12]$, the inferred SGWB amplitude is therefore strongly peaked toward the upper edge of the prior, reflecting the fact that part of the low-frequency power is absorbed by the red noise, while the remaining contribution is ascribed to the SGWB. This behavior, often referred to as the *red noise–SGWB degeneracy* (e.g. van Haasteren and Vallisneri, 2014; EPTA Collaboration et al., 2023), motivates the introduction of a hierarchical description of the noise model, which allows us to capture the population-level variability of the noise parameters and to mitigate prior-driven projection effects, as we will show below.

Beyond this global interplay between red-noise and SGWB amplitudes, the posteriors also exhibit the well-known anticorrelation correlation between the spectral index and the logarithmic amplitude, typical of each power-law processes, see e.g. Lentati et al. (2016); Taylor (2021). This negative correlation arises from the degeneracy in the power-law spectrum $P(f) \propto A^2 f^{-\gamma}$: for a given dataset, a steeper spectral index (larger γ) can be compensated by a higher amplitude A , and vice versa. The effect is particularly evident for the SGWB, whose amplitude and spectral index show elongated, anti-correlated posterior contours. The same qualitative behaviour is observed for the DM variation noise parameters $(\log_{10} A_{\text{dm}}, \gamma_{\text{dm}})$, although it is mitigated by the additional frequency dependence f^{-2} characteristic of chromatic processes: since DM variations imprint a dispersive delay that scales with the inverse squared observing frequency, multi-frequency data provide an extra constraint that partially breaks the degeneracy between amplitude and spectral index.

Figure 3 further shows that the SGWB amplitude is not only sharply peaked but also displaced from the injected value. This bias arises from the combined effect of the red-noise–SGWB degeneracy and the limited size of the array: with only 3 pulsars, part of the red-noise power is absorbed into the common SGWB component, producing an overestimated amplitude and a slightly biased spectral index. This behavior underscores the need for a hierarchical treatment of the noise parameters.

4.1. Adding hierarchical description of the noise

We now include a hierarchical layer in the noise modeling by placing Gaussian hyperpriors on the lower and upper bounds of the red-noise and DM-variation priors. The means and standard deviations of these hyperpriors are taken from the inference reported in Table 2 of Goncharov and Sardana (2025), ensuring consistency with population-level noise statistics derived from the EPTA dataset. The comparison with the non-hierarchical runs immediately highlights three main effects.

First, the red-noise parameters become more constrained: their marginal posteriors in Figure 5 are noticeably less flat than in the fixed-prior case, indicating that the hierarchical structure effectively regularizes the wide uniform priors. Second, the corner plot in Figure 4a shows that the characteristic anticorrelation between $\log_{10} A$ and γ begins to emerge also for the red-noise component, confirming that the additional hierarchical layer helps recover physically meaningful

Marginal posterior of physical parameters for J1744–1134 without hyperpriors

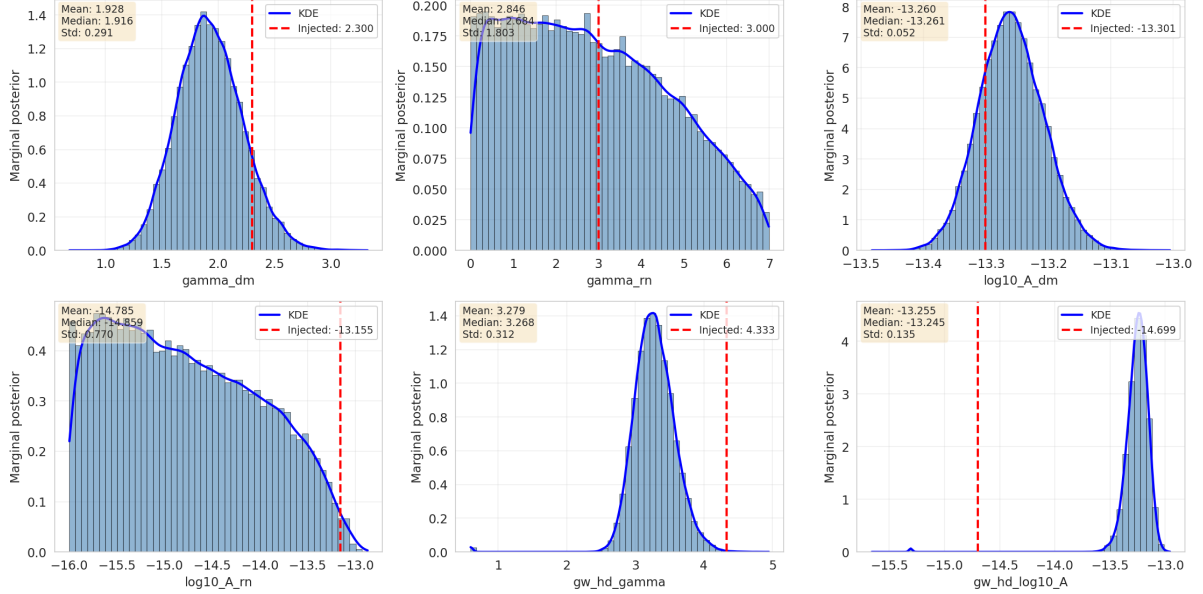


Figure 3: Marginal posterior distributions for the noise and SGWB parameters of pulsar J1744–1134 obtained with fixed uniform priors. The red vertical lines indicate the injected values. The sharp upper-edge peak of the SGWB amplitude posterior primarily reflects the prior-bound effect, but is also reinforced by the limited number of pulsars and by the intrinsic red-noise–SGWB degeneracy. This behaviour is particularly evident in small arrays, where the Hellings–Downs correlation drives the sampler to attribute most of the frequency power to the common SGWB component.

parameter dependencies that were previously washed out by the lack of constraints. Third, and perhaps most interestingly, the SGWB parameters appear essentially unaffected by the introduction of hyperpriors on the noise. At least within this minimal three-pulsar configuration, the hierarchical treatment of the noise has negligible impact on the inferred SGWB amplitude and spectral index.

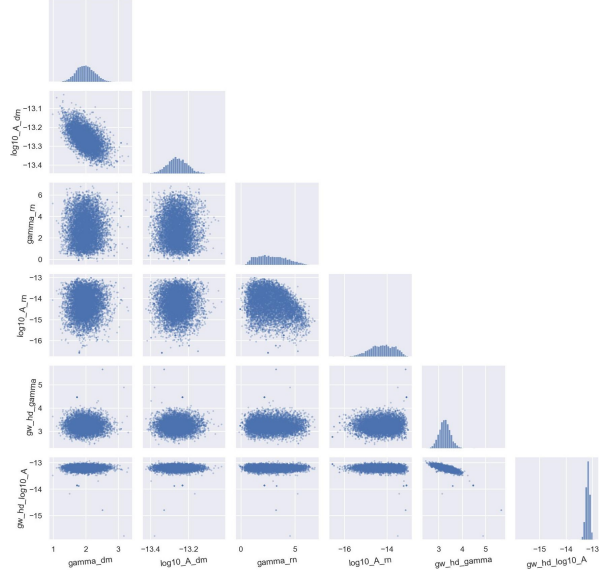
This conclusion is supported by the detailed parameter–hyperparameter correlation analysis based on the independence score metric $\mathcal{I}(\vartheta_i, \Lambda_j)$ defined as

$$\mathcal{I}(\vartheta_i, \Lambda_j) = \frac{\mathbb{E}[\text{Var}(\vartheta_i | \Lambda_j)]}{\text{Var}(\vartheta_i)} \quad (5)$$

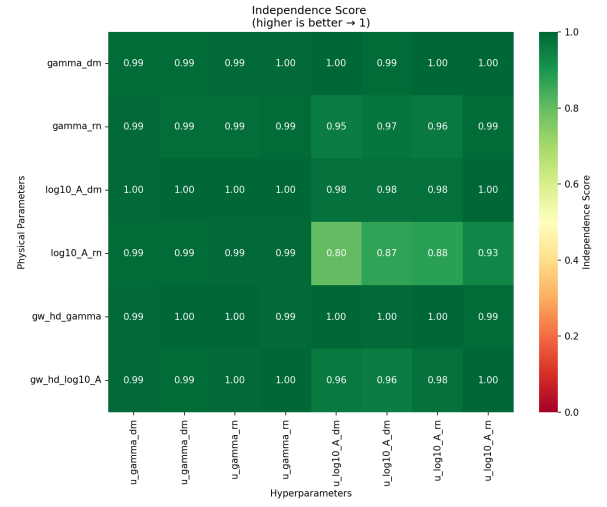
and ranging from 0 to 1, with values approaching 1 indicating that ϑ_i is largely independent of Λ_j . This metric quantifies the fraction of variance in the physical parameter that is not explained by the hyperparameter, thus measuring the degree of statistical independence. As visible in Figure 4b, the SGWB parameters ($\log_{10} A_{\text{GWB}}$, γ_{GWB}) are practically independent of the noise hyperparameters, especially γ_{GWB} . Conversely, the noise hyperparameters display mild correlations with their corresponding physical parameters, as expected from the hierarchical coupling. Overall, these results suggest that the limited size of the array and the strong red-noise–SGWB degeneracy discussed in the previous section may dominate over the hierarchical effects, at least for the SGWB component in this small-PTA setting.

4.2. The effects of the decorrelation

We now examine the results obtained after applying the orthogonal projection that decorrelates the hyperparameters, as described in Section 3.1. Figure 6b shows the dependencies between the



(a) Corner plot showing the 2D-joint posterior distributions of the noise and SGWB parameters for pulsar J1744–1134 under hierarchical noise modeling with Gaussian hyperpriors. The red-noise parameters now display a clearer anticorrelation between $\log_{10} A$ and γ , while the SGWB contours remain nearly identical to the fixed-prior case, confirming that the hierarchical treatment primarily affects the noise sector in this minimal 3-pulsar setup.



(b) Independence score metric values introduced by the hierarchical treatment of the noise before decorrelation. All noise parameters display a mild interplay while the SWGB results to be almost uncorrelated.

Figure 4: Corner plot of the noise and SGWB parameters (left) and independence score metric for the correlations between the physical and hyperparameters for pulsar J1744–1134 with a hierarchical treatment of the noise

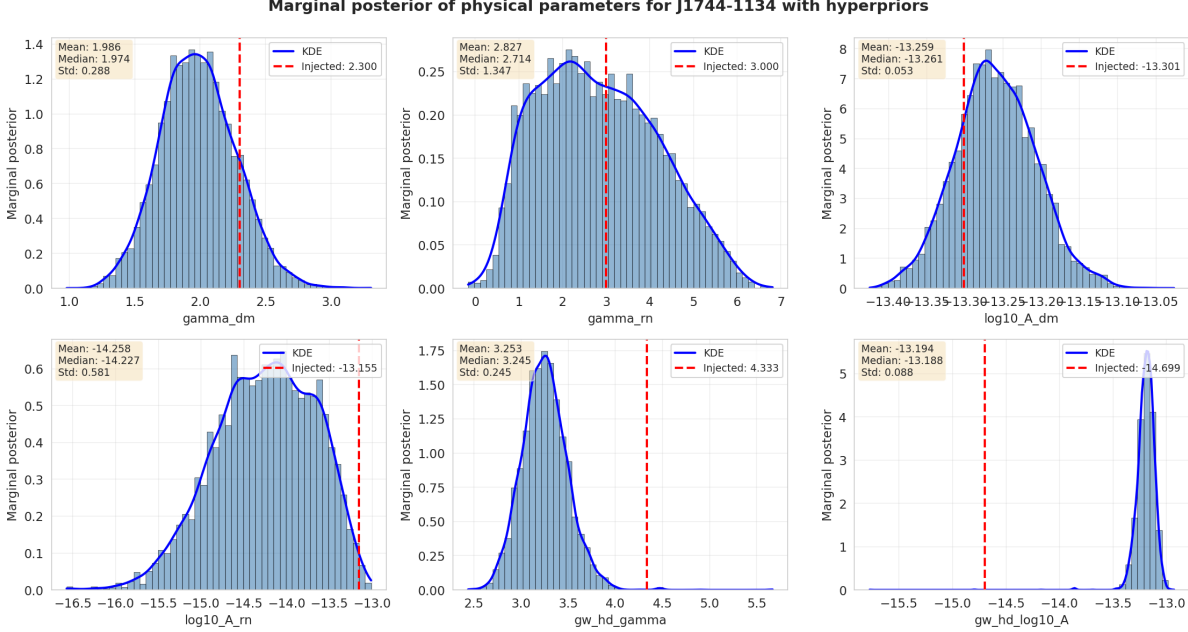
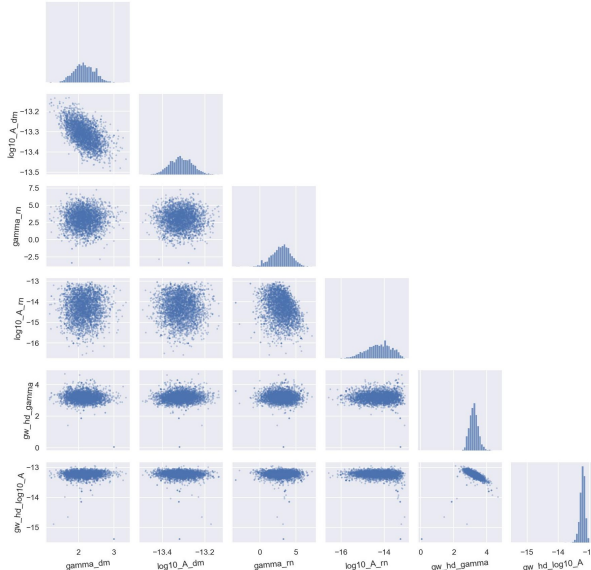


Figure 5: Marginal posterior distributions for the noise and SGWB parameters of pulsar J1744–1134 obtained with Gaussian hyperpriors on the red-noise and DM-variation priors. The red vertical lines mark the injected values. Compared to the fixed-prior case, the red-noise posteriors are more constrained, while the SGWB parameters remain largely unchanged, indicating that in this small-array configuration the hierarchical treatment mainly regularizes the noise components.

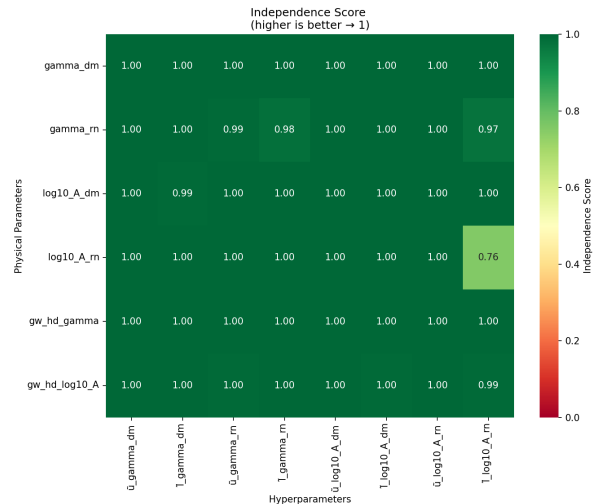
physical parameters and the transformed hyperparameters. After reparametrization, all parameters become effectively independent, confirming that the projection successfully removes correlations introduced by the hierarchical prior. The only exception is $\log_{10} A_{\text{rn}}$, which remains mildly correlated - a residual feature already present in the original parameterization and consistent with the intrinsic difficulties of constraining the red-noise amplitude in small arrays. At the same time, Figures 6a and 7 show that the red-noise parameters are now even better constrained, and that the anticorrelation between $\log_{10} A_{\text{rn}}$ and γ_{rn} becomes more pronounced. Taken together, these results indicate that the orthogonal projection effectively disentangles correlations arising from the hierarchical structure itself, removing spurious hyperprior dependencies while enhancing the genuine power-law relationships that characterize the noise processes modeling. As in the previous cases, the SGWB parameters remain essentially unaffected, further confirming that, within this minimal 3-pulsar configuration, the hierarchical and reparametrized treatments primarily influence the noise sector.

5. Concluding remarks and future directions

In this work, we have developed a hierarchical Bayesian framework for PTA noise modeling that addresses the fundamental issue of prior sensitivity. The starting point is the introduction of hyperpriors on pulsar noise parameters, which elevates the problem to a hierarchical setting where hyperparameters themselves play the role of nuisance parameters. To handle the correlations between hyperparameters and physical noise parameters, we implemented an orthogonal reparameterization strategy based on a two-step Normalizing Flows algorithm. The algorithm learns the transformation that removes the projection of hyperparameters onto the subspace spanned by the physical parameters, thus producing a decorrelated set of hyperparameters as the orthogonal



(a) Corner plot showing the 2D-joint posterior distributions of the noise and SGWB parameters for pulsar J1744–1134 after hyperparameters decorrelation. The red-noise parameters now display a clearer anti-correlation between $\log_{10} A$ and γ , while the SGWB contours remain nearly identical to the correlated case.



(b) Independence score metric values after hyperparameters decorrelation. All physical parameters are now effectively independent of their corresponding hyperparameters, except for a mild residual correlation in $\log_{10} A_{rn}$, consistent with the intrinsic difficulty of constraining the red-noise amplitude in small arrays.

Figure 6: Corner plot of the noise and SGWB parameters (left) and independence score metric for the correlations between the physical and hyperparameters for pulsar J1744–1134 after hyperparameters decorrelation

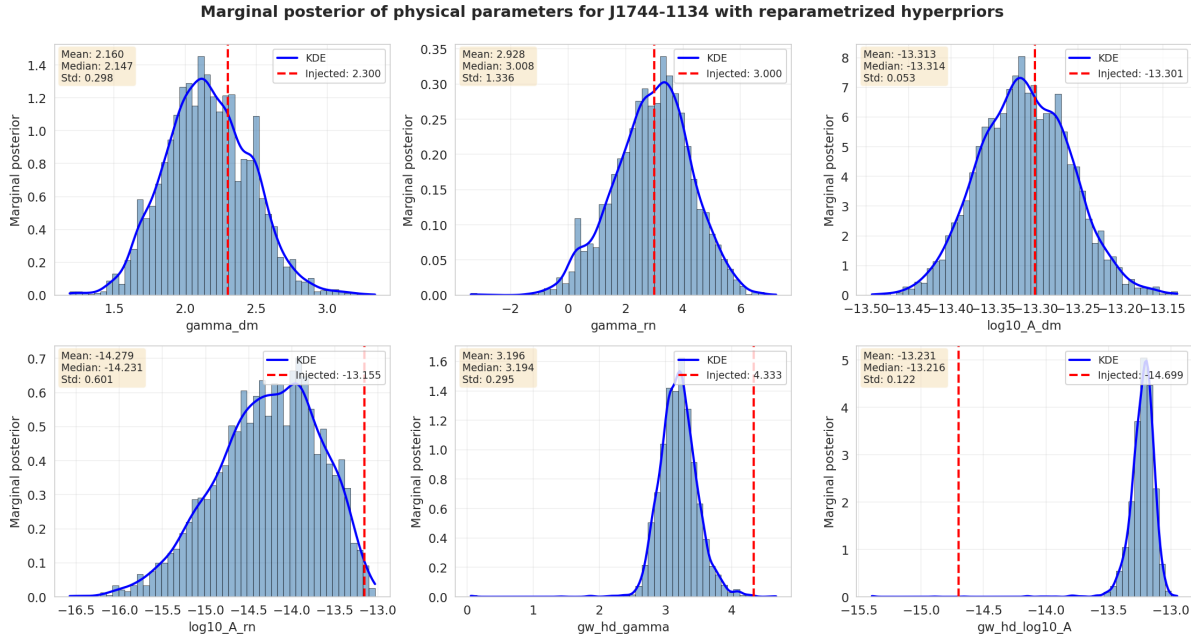


Figure 7: Marginal posterior distributions for the noise and SGWB parameters of pulsar J1744–1134 after hyperparameter decorrelation. The red vertical lines mark the injected values. Compared to the hierarchical but non-decorrelated case, the red-noise posteriors are further tightened, while the SGWB parameters remain unchanged, confirming that the orthogonal projection primarily refines the noise inference without affecting the common signal.

complement. This reparametrization strategy ensures, in principle, that the inference on signal parameters becomes less sensitive to the specific choice of noise priors.

Bayesian inference was performed using **i-nessai**, a flow-based nested sampling algorithm that, integrated in **Enterprise**, significantly accelerates the inference pipeline compared to traditional PTMCMC samplers while maintaining robust posterior and evidence estimation, as shown in Villa et al. (2025). We applied this framework to a minimal simulated dataset consisting of 3 pulsars, performing a simultaneous inference of noise and SGWB parameters. Although such a small array is not at all sufficient for a fully representative PTA analysis, it provides a controlled and transparent proof of concept that allows us to isolate and assess the key effects of the hierarchical modeling and reparametrization.

Our analyses - including corner plots, marginal posteriors, and parameter–hyperparameter correlation metric - consistently show the same qualitative picture. Even with only 3 pulsars, where the overall constraining power is limited, we find that: (i) introducing the statistical distribution of the noise parameters through Gaussian hyperpriors partially breaks the red-noise–SGWB degeneracy, leading to a more stable inference of the noise components (ii) decorrelating physical and hyperparameters via orthogonal projection further improves the constraints, revealing the expected $\log_{10} A - \gamma$ anticorrelation for the red noise. The SGWB parameters, instead, remain only weakly constrained, as expected given the limited number of pulsars.

In summary, this study represents a first application of our hierarchical and reparametrized framework to PTA data analysis. Although the present configuration serves primarily as a methodological test, the results clearly demonstrate the potential of the approach for reducing prior dependence and improving the interpretability of hierarchical PTA models. Future work will explore its application to larger arrays and to real PTA datasets, where the combined effects of hierarchy and reparametrization can be fully exploited to achieve more robust and physically meaningful inferences on the SGWB.

Acknowledgements

This paper is supported by the Fondazione ICSC, Spoke-3 Astrophysics and Cosmos Observations, National Recovery and Resilience Plan (Piano Nazionale di Ripresa e Resilienza, PNRR) Project ID CN_00000013 “Italian Research Center on High-Performance Computing, Big Data and Quantum Computing” funded by MUR Missione 4 Componente 2 Investimento 1.4: Potenziamento strutture di ricerca e creazione di “campioni nazionali di R&S (M4C2-19)” - Next Generation EU (NGEU).

We acknowledge the Istituto Nazionale di Astrofisica (INAF) computing time allocation award under the the proposal *FastParam* for the *PLEIADI* computing infrastructure initiative. The HPC tests and benchmarks of this work have been carried out on the cluster *PLEIADI*, installed and managed by INAF. The cluster we used is equipped with dual Intel Xeon E5-2697 V4 processors (36 cores per node) and 128 GB of RAM. For this work, all jobs were executed on a single node using 1 CPU core and 128 GB of RAM, via the SLURM scheduler within the *large* partition.

The authors thank Romina T. Anfuso, Project Manager at Koexai srl, for project management support and coordination.

E.V. thanks Marco Bonici for insightful discussions about our reparametrization approach compared to the one in Paradiso et al. (2025).

Declaration of generative AI and AI-assisted technologies in the manuscript preparation process

During the preparation of this work, the authors used chatGPT5 to correct grammar misspellings, consistency of notation and terminology, and language fluency. After using this tool/service, the authors reviewed and edited the content as needed and assume full responsibility for the content of the published article.

References

Agazie, G., Anumarlapudi, A., Archibald, A.M., et al., 2023. The nanograv 15 yr data set: Evidence for a gravitational-wave background. *The Astrophysical Journal Letters* 951, L8. doi:10.3847/2041-8213/acdac6, arXiv:2306.16213.

Christensen, O.F., Roberts, G.O., Sköld, M., 2006. Robust markov chain monte carlo methods for spatial generalized linear mixed models. *Journal of Computational and Graphical Statistics* 15, 1–17.

collaboration, E., Collaboration, I., Antoniadis, J., Babak, S., Nielsen, A.S.B., Bassa, C.G., Berthureau, A., Bonetti, M., Bortolas, E., Brook, P.R., Burgay, M., Caballero, R.N., Chalumeau, A., Champion, D.J., Chanlaridis, S., Chen, S., Cognard, I., Desvignes, G., Falxa, M., Ferdinand, R.D., Franchini, A., Gair, J.R., Goncharov, B., Graikou, E., Grießmeier, J.M., Guillermot, L., Guo, Y.J., Hu, H., Iraci, F., Izquierdo-Villalba, D., Jang, J., Jawor, J., Janssen, G.H., Jessner, A., Karuppusamy, R., Keane, E.F., Keith, M.J., Kramer, M., Krishnakumar, M.A., Lackeos, K., Lee, K.J., Liu, K., Liu, Y., Lyne, A.G., McKee, J.W., Maan, Y., Main, R.A., Mickaliger, M.B., Nitu, I.C., Parthasarathy, A., Perera, B.B.P., Perrodin, D., Petiteau, A., Porayko, N.K., Possenti, A., Quelquejay-Leclere, H., Samajdar, A., Sanidas, S.A., Sesana, A., Shaifullah, G., Speri, L., Spiewak, R., Stappers, B.W., Susarla, S.C., Theureau, G., Tiburzi, C., van der Wateren, E., Vecchio, A., Krishnan, V.V., Verbiest, J.P.W., Wang, J., Wang, L., Wu, Z., 2023. The second data release from the european pulsar timing array i. the dataset and timing analysis. *Astronomy & Astrophysics* 678, A48. URL: <https://arxiv.org/abs/2306.16224>, doi:10.1051/0004-6361/202346841, arXiv:2306.16224.

Cox, D.R., Reid, N., 1987. Parameter orthogonality and approximate conditional inference. *Journal of the Royal Statistical Society. Series B (Methodological)* 49, 1–39.

D’Amico, L., Villa, E., et al., 2025. Addressing prior dependence in hierarchical bayesian modeling for pta data analysis i: Methodology and implementation, in: *Proceedings of the 28th International Supercomputing Conference (ISC 2025)*, Springer. Under review.

EPTA Collaboration, InPTA Collaboration, Antoniadis, J., et al., 2023. The second data release from the european pulsar timing array. iii. search for gravitational wave signals. *Astronomy & Astrophysics* 678, A50. doi:10.1051/0004-6361/202346844, arXiv:2306.16214.

Goncharov, B., Sardana, S., 2025. Ensemble noise properties of the european pulsar timing array. *Monthly Notices of the Royal Astronomical Society* 537, 3470–3479. URL: <http://dx.doi.org/10.1093/mnras/staf190>, doi:10.1093/mnras/staf190.

van Haasteren, R., 2024a. Pulsar timing arrays require hierarchical models. *The Astrophysical Journal Supplement Series* 273, 23. URL: <http://dx.doi.org/10.3847/1538-4365/ad530f>, doi:10.3847/1538-4365/ad530f.

van Haasteren, R., 2024b. Use model averaging instead of model selection in pulsar timing. *Monthly Notices of the Royal Astronomical Society: Letters* 537, L1–L6. URL: <http://dx.doi.org/10.1093/mnrasl/slae108>, doi:10.1093/mnrasl/slae108.

van Haasteren, R., Vallisneri, M., 2014. Gravitational wave detection using pulsar timing arrays. *Monthly Notices of the Royal Astronomical Society* 446, 1170–1174. URL: <https://doi.org/10.1093/mnras/stu2159>, doi:10.1093/mnras/stu2159.

Kobyzev, I., Prince, S.J., Brubaker, M.A., 2021. Normalizing flows: An introduction and review of current methods. *IEEE Transactions on Pattern Analysis and Machine Intelligence* 43, 3964–3979. URL: <http://dx.doi.org/10.1109/TPAMI.2020.2992934>, doi:10.1109/tpami.2020.2992934.

Laal, N., Taylor, S.R., van Haasteren, R., Lamb, W.G., Siemens, X., 2025. Solving the pta data analysis problem with a global gibbs scheme. *Physical Review D* 111. URL: <http://dx.doi.org/10.1103/PhysRevD.111.063067>, doi:10.1103/physrevd.111.063067.

Lentati, L., Shannon, R.M., Coles, W.A., van Haasteren, R., Ellis, J.A., Taylor, S.R., Hobbs, G., Janssen, G.H., Manchester, R.N., Reardon, D.J., et al., 2016. Wide-band profile domain pulsar timing analysis. *Monthly Notices of the Royal Astronomical Society* 458, 2161–2187. URL: <https://doi.org/10.1093/mnras/stw395>, doi:10.1093/mnras/stw395.

Papamakarios, G., Pavlakou, T., Murray, I., 2017. Masked autoregressive flow for density estimation, in: *Advances in Neural Information Processing Systems*.

Papaspiliopoulos, O., Roberts, G.O., Sköld, M., 2007. A general framework for the parametrization of hierarchical models. *Statistical Science* 22, 59–73.

Paradiso, S., Bonici, M., Chen, M., Percival, W., D’Amico, G., Zhang, H., McGee, G., 2025. Reducing nuisance prior sensitivity via non-linear reparameterization, with application to eft analyses of large-scale structure. *Journal of Cosmology and Astroparticle Physics* 2025, 005. URL: <http://dx.doi.org/10.1088/1475-7516/2025/07/005>, doi:10.1088/1475-7516/2025/07/005.

Reardon, D.J., Zic, A., Shannon, R.M., et al., 2023. Search for an isotropic gravitational-wave background with the parkes pulsar timing array. *The Astrophysical Journal Letters* 951, L6. doi:10.3847/2041-8213/acdd02, arXiv:2306.16215.

Rezende, D.J., Mohamed, S., 2015. Variational inference with normalizing flows, in: Bach, F., Blei, D. (Eds.), *Proceedings of the 32nd International Conference on Machine Learning*, PMLR, Lille, France. pp. 1530–1538.

Taylor, S.R., 2021. The nanohertz gravitational wave astronomer. URL: <https://arxiv.org/abs/2105.13270>, arXiv:2105.13270.

Thrane, E., Talbot, C., 2019. An introduction to Bayesian inference in gravitational-wave astronomy: Parameter estimation, model selection, and hierarchical models. *PASA* 36, e010. doi:10.1017/pasa.2019.2, arXiv:1809.02293.

Tibshirani, R., Wasserman, L., 1994. Some aspects of the reparametrization of statistical models. *The Canadian Journal of Statistics* 22, 163–173.

Trippe, B.L., Turner, R.E., 2018. Conditional density estimation with bayesian normalising flows. arXiv preprint arXiv:1802.04908 .

Villa, E., Shaifullah, G., Possenti, A., Carbone, C., 2025. Improving bayesian inference in pta data analysis: importance nested sampling with normalizing flows. *Astronomy and Computing*, Submitted.

Williams, M.J., 2021. nessai: Nested sampling with artificial intelligence. URL: <https://doi.org/10.5281/zenodo.4550693>, doi:10.5281/zenodo.4550693.

Williams, M.J., Veitch, J., Messenger, C., 2021. Nested sampling with normalizing flows for gravitational-wave inference. *Physical Review D* 103. URL: <http://dx.doi.org/10.1103/PhysRevD.103.103006>, doi:10.1103/physrevd.103.103006.

Williams, M.J., Veitch, J., Messenger, C., 2023. Importance nested sampling with normalising flows. *Machine Learning: Science and Technology* 4, 035011. URL: <http://dx.doi.org/10.1088/2632-2153/acd5aa>, doi:10.1088/2632-2153/acd5aa.

Xu, H., Chen, S., Guo, Y., Jiang, J., Wang, B., Xu, J., Xue, Z., Caballero, R.N., et al., 2023. Searching for the nano-hertz stochastic gravitational wave background with the chinese pulsar timing array data release i. *Research in Astronomy and Astrophysics* 23, 075024. doi:10.1088/1674-4527/acdfa5, arXiv:2306.16216.